Solution of the vector wave equation by the separable effective adiabatic basis set method

Kirill Gokhberg, Ilya Vorobeichik, and Edvardas Narevicius

OpTun Ltd., MTM Scientific Industries Center, Haifa 31905, Israel

Nimrod Moiseyev

OpTun Ltd., MTM Scientific Industries Center, Haifa 31905, Israel, and Department of Chemistry and Minerva Center for Non-Linear Physics of Complex Systems, Technion–Israel Institute of Technology, Haifa 32000, Israel

Received July 31, 2003; revised manuscript received March 14, 2004; accepted April 8, 2004

A novel separable effective adiabatic basis (SEAB) for the solution of the transverse vector wave equation by the variational method is presented. The basis is constructed by a suitably modified adiabatic approximation. The method of SEAB construction is applicable to the waveguides of a general cross section. By calculating scalar modes in rectangular and rib waveguides, we show that the use of SEAB entails computational effort several orders of magnitude less than the use of the more conventional Fourier basis. As an illustrative example, the polarized modes of a rib waveguide are calculated. © 2004 Optical Society of America

OCIS codes: 190.4420, 230.7370, 000.3860.

1. INTRODUCTION

Solution of the scalar wave equation in dielectric waveguide structures is frequently sufficient to develop and analyze photonic devices. However, to determine such characteristics of the device as polarization-dependent loss and polarization-mode-dispersion knowledge of the vector modes and their propagation constants is essential. A number of methods have been developed so far to solve two-dimensional vector wave equations in the dielectric waveguides. Approximate solutions can be obtained in a fast and efficient way by the effective-index method with perturbative treatment of polarization corrections.[1,2] To go beyond the approximate solutions and to obtain vector modes with any degree of accuracy, researchers have extensively used the variational approach. The Ritz variational method was utilized in Refs. 3 and 4 to find scalar modes and then to compute polarization corrections by the perturbation theory. The Ritz–Galerkin variational method, wherein the original Sturm–Liouville problem is replaced by the equivalent matrix eigenvalue problem, has been extensively used to find scalar and semivectorial modes in waveguides.[5–7] However, to the best of our knowledge, it was never implemented to solve the full vector equation.

One of the factors affecting performance of the variational method is the choice of the trial or basis functions. Obviously, if they closely resemble the exact solutions, i.e., if they are physical functions, then the amount of numerical work needed to represent the exact solutions with sufficient precision is not large. Thus the use of Hermite–Gauss basis functions in Refs. 8 and 9 allowed the accurate representation of the bound modes in circular and rectangular waveguides with just a few basis functions and therefore cut computational costs. However, such hand picked bases are not portable between waveguides with widely different cross sections. This explains the widespread use of the more flexible, although unphysical, Fourier basis.

In this paper we demonstrate how the full vector equation can be solved by the variational method. To this end, we use the suitably modified adiabatic (effective-index) method to construct a physical separable basis suitable for waveguides with a cross section of any form.

Although the Fourier basis is used to represent our basis functions, we obtain numerical solutions of the vector equations that can contain as many as 10^6 Fourier components. The use of a Fourier basis of such size directly would represent a much more difficult numerical task. The computational efficiency of the proposed basis versus the Fourier basis is demonstrated in the solution of the proposed basis, and is consequently used to calculate vector modes in the same waveguide structures, whereby a high precision of computation is shown to be achieved with a reasonable amount of basis functions.

2. PHYSICAL PROBLEM

To obtain vector modes of straight dielectric waveguides, one must solve the complete set of Maxwell equations. Assuming the fields to be time harmonic and eliminating the magnetic field, we arrive at the equivalent set of equations

$$\nabla \times \nabla \times \mathbf{E}(\mathbf{r}) - \frac{\omega^2}{c^2} n^2(\mathbf{r}) \mathbf{E}(\mathbf{r}) = 0, \tag{1}$$

$$\nabla \cdot \mathbf{E}(\mathbf{r}) = -\mathbf{E}(\mathbf{r}) \cdot \nabla[\ln n^2(\mathbf{r})], \tag{2}$$

where $\mathbf{E}(\mathbf{r})$ is the electric field and $n(\mathbf{r})$ is the refractive index. We choose the z axis to be along the waveguide;

 © 2004 Optical Society of America

thus $n(\mathbf{r}) \equiv n(x, y)$ is independent of z, and the electric field can be written in the form $\mathbf{E}(\mathbf{r}) = \mathbf{E}(x, y)\exp(i\beta z)$, where β is the propagation constant and $\mathbf{E}(x, y)$ is the vector mode. By substituting the above expression for the electric field into Eqs. (1) and (2), we obtain the following equation for the vector mode $\mathbf{E}(x, y)$:

$$\begin{bmatrix} \nabla_\perp^2 + k^2 n^2(x, y) + f_x \frac{\partial}{\partial x} + f_{xx} - \beta^2 & f_y \frac{\partial}{\partial x} + f_{xy} & 0 \\ f_x \frac{\partial}{\partial y} + f_{xy} & \nabla_\perp^2 + k^2 n^2(x, y) + f_y \frac{\partial}{\partial y} + f_{yy} - \beta^2 & 0 \\ i\beta f_x & i\beta f_y & \nabla_\perp^2 + k^2 n^2(x, y) - \beta^2 \end{bmatrix} \mathbf{E}(x,y) = 0, \quad (3)$$

where $k = \omega/c$ is the free-space wave vector, $f = 2 \ln n(x, y)$, and subscripts denote the partial derivatives. Solution of Eq. (3) should produce real propagation constants β. This can be deduced from Berry's representation of the Maxwell equations for guided light as a Schrödinger-like equation.[10] We see from Eq. (2) that if the variations in the refractive index are small then the field becomes nearly transversal; i.e., $E_z(x, y)$ is much smaller than the transversal component $\mathbf{E}_\perp(x, y)$. Therefore we might neglect the z component of the field and rewrite Eq. (3) as an eigenvalue problem for the transverse component of the field alone:

$$\hat{\Theta}\mathbf{E}_\perp(x, y) = \beta^2 \mathbf{E}_\perp(x, y). \quad (4)$$

The operator $\hat{\Theta}$ is given by

$$\hat{\Theta} = \begin{bmatrix} \nabla_\perp^2 + k^2 n^2(x, y) & 0 \\ 0 & \nabla_\perp^2 + k^2 n^2(x, y) \end{bmatrix} + \begin{bmatrix} f_x \frac{\partial}{\partial x} + f_{xx} & f_y \frac{\partial}{\partial x} + f_{xy} \\ f_x \frac{\partial}{\partial y} + f_{xy} & f_y \frac{\partial}{\partial y} + f_{yy} \end{bmatrix}. \quad (5)$$

The transverse component of the mode is an eigenfunction of $\hat{\Theta}$ while the second power of the propagation constant is its eigenvalue. We see that in this approach the solution of the full set of Maxwell equations is reduced to the determination of eigenfunctions and eigenvalues of the operator given in Eq. (5).

We define the scalar product between fields $\mathbf{E_1}$ and $\mathbf{E_2}$ in the following way (see Ref. 11):

$$\langle \mathbf{E_1} | \mathbf{E_2} \rangle = \frac{1}{i} \int (\mathbf{E_1}^* \times \nabla \times \mathbf{E_2} - \mathbf{E_2} \times \nabla \times \mathbf{E_1}^*)_z dx dy. \quad (6)$$

In the case $\mathbf{E_1} = \mathbf{E_2} = \mathbf{E}$, the scalar product in Eq. (6) becomes proportional to the total power in the mode $\mathbf{E}$. In our approximation, when the z component of the field is neglected, the scalar product takes a simpler form:

$$\langle \mathbf{E_1} | \mathbf{E_2} \rangle = \int \mathbf{E}_{\perp,1}^* \mathbf{E}_{\perp,2} dx dy. \quad (7)$$

Operator $\hat{\Theta}$ is, in general, non-Hermitian, which may result in nonphysical complex propagation constants. The fact that Eq. (4) is a non-Hermitian eigenvalue problem is not in conflict with the hermeticity of Maxwell equations. Only because of the assumption that $E_z(x, y)$ is negligible compared with the transversal component $\mathbf{E}_\perp$ have we arrived at the non-Hermitian operator $\hat{\Theta}$ in Eq. (4). It is important to stress that the non-Hermitian nature of $\hat{\Theta}$ is due to the approximation we made.

In view of the non-Hermitian nature of $\hat{\Theta}$, we redefine the scalar product in the functional space of vectors $\mathbf{E}_\perp$ as

$$(\mathbf{E}_\perp^L | \mathbf{E}_\perp^R) = \int dx dy \mathbf{E}_\perp^L \cdot \mathbf{E}_\perp^R, \quad (8)$$

where $\mathbf{E}_\perp^L$ and $\mathbf{E}_\perp^R$ are left and right eigenfunctions of $\hat{\Theta}$ (e.g., see Ref. 12).

3. COMPLEX VARIATIONAL METHOD

To find eigenfunctions and eigenvalues of $\hat{\Theta}$, we used a complex analog of the variational principle proved in Ref. 12. In this method, eigenfunctions of $\hat{\Theta}$ are represented as an expansion in the N linearly independent basis functions χ_i. If normalized eigenfunctions of some Hermitian operator are chosen as the basis, then such a basis is orthonormal, and the relation $\chi_i^L = \chi_i^{R*} \equiv \chi_i^*$ holds. Consequently, the right and left eigenfunctions of $\hat{\Theta}$ are of the form

$$|\mathbf{E}_\perp^R\rangle = \sum_{j=1}^N C_j^R \chi_j,$$

$$\langle \mathbf{E}_\perp^L| = \sum_{j=1}^N C_j^L \chi_j^*. \quad (9)$$

The variational principle states that the expansion coefficients C_j^R are solutions of the following matrix eigenvalue problem:

$$\sum_{j=1}^N C_j^R (\Theta_{ij} - \bar{E} S_{ij}) = 0, \quad (10)$$

where $\Theta_{ij} = (\chi_i|\hat{\Theta}|\chi_j)$ is the matrix element of the operator in question and $S_{ij} = (\chi_i|\chi_j) = \delta_{ij}$. Coefficients C_j^L are found in a similar fashion with transposed matrix Θ_{ij}^t substituted into Eq. (10) instead of Θ_{ij}. The variational principle also ensures that in the limit $N \to \infty$ expansions (9) approach the exact eigenfunctions of $\hat{\Theta}$.

In numerical calculations the number of the basis functions N is necessarily finite. Thus the choice of basis becomes of paramount importance to ensure the fast convergence of expansions (9), thus minimizing the size of matrices fed into the diagonalization procedure. A widespread choice is the Fourier basis, separable in coordinates x and y, which often enables one to obtain the matrix elements Θ_{ij} in an analytical form and save the time necessary for its numerical evaluation. However, the basis functions are unphysical; i.e., they bear little resemblance to the modes. One might expect in this case that very large N's are needed to obtain satisfactory convergence. We demonstrate below an efficient method to construct a separable physical basis whose functions resemble closely the exact waveguide modes.

4. SEPARABLE EFFECTIVE ADIABATIC BASIS

We will obtain the desired basis functions solving the scalar wave equation

$$\left[\frac{\partial^2}{\partial x^2} + \frac{\partial^2}{\partial y^2} + k^2 n^2(x, y) - \beta^2\right]\phi(x, y) = 0 \quad (11)$$

by the suitably modified adiabatic method that will be introduced below. (For a detailed discussion of the standard adiabatic approximation, known in optics as the effective-index method, consult Ref. 13 or 14). Application of the adiabatic method alone produces an excellent approximation to the solutions of Eq. (11). However, these solutions are neither separable nor continuous for the piece wise potentials as in the case we want to study; thus they are not a convenient choice as the basis functions. Nevertheless, by modifying the adiabatic approximation, we will be in a position to obtain a separable basis whose functions are continuous and similar to the exact solutions.

We define a box in the xy plane and introduce the grid with N_x points in the x direction and N_y points in the y direction. We denote by L_x and L_y characteristic dimensions of the waveguide in the x and y directions correspondingly. If characteristic dimension L_x is larger than L_y (extension to the case when $L_x < L_y$ is obvious), then the variation of $\phi(x, y)$ with x is slower than with y. In this case the term $\partial^2\phi(x, y)/\partial x^2$ in Eq. (11) can be regarded as a small perturbation. Treating coordinate x as a parameter, we solve the following Hermitian eigenvalue equation for some functions $Y_m(y; x)$:

$$\left[\frac{\partial^2}{\partial y^2} + k^2 n^2(x, y)\right]Y_m(y; x) = \beta_m{}^2(x) Y_m(y; x), \quad (12)$$

where $\beta_m(x) = kn_m(x)$, $m = 1,...N_y$, defines the effective refractive index of the medium in the x direction. Equation (12) is solved numerically for each x. To this end, we utilized the Hermitian variational (Ritz) method with N_y Fourier basis functions and periodic boundary conditions. As the next step, we should solve N_y eigenvalue problems for the slow coordinate, x, by use of N_y different functions $\beta_m(x)$:

$$\left[\frac{\partial^2}{\partial x^2} + \beta_m{}^2(x)\right]X_{nm}(x) = (\beta_{nm}{}^{\mathrm{ad}})^2 X_{nm}(x). \quad (13)$$

Adiabatic solutions of Eq. (11) are $\phi_{nm}{}^{\mathrm{ad}} = X_{nm}(x)Y_m(y; x)$, and $(\beta_{nm}{}^{\mathrm{ad}})^2$ are the adiabatic eigenvalues.

Although they are a close approximation to the exact solutions, adiabatic functions are inconvenient as a basis, since they are neither separable nor continuous. To obtain a more suitable basis, we modify the above procedure in the following way. We choose only one effective refractive index, $\beta_1(x) = kn_1(x)$, and the following equation is solved:

$$\left[\frac{\partial^2}{\partial x^2} + \beta_1{}^2(x)\right]X_{i1}(x) = (\beta_{i1}{}^{\mathrm{ad}})^2 X_{i1}(x). \quad (14)$$

To obtain N_x eigenfunctions $X_{i1}(x) \equiv X_i(x)$, we use the variational Ritz method with N_x Fourier basis functions and periodic boundary conditions. We represent the desired separable basis as $X_i(x)Y_j(y)$, where $Y_j(y)$'s are yet to be found. To determine $Y_j(y)$'s, we substitute $X_1(x)Y_j(y)$ into Eq. (11), multiply from the left by $X_1{}^*(x)$, and integrate over x. As a result, we obtain the effective Hermitian eigenvalue problem

$$\left[\frac{\partial^2}{\partial y^2} + \beta^2(y) - \beta_j{}^2\right]Y_j(y) = 0, \quad (15)$$

where $\beta(y) = kn(y)$ defines the effective refractive index in the y direction and is given by

$$\beta^2(y) = (\beta_{11}{}^{\mathrm{ad}})^2 + \int dx X_1(x)^*[k^2 n^2(x, y) - \beta_1{}^2(x)]X_1(x). \quad (16)$$

Note that here we add and subtract in the right-hand side of Eq. (11) the term $\beta_1{}^2(x)$ in order to simplify the calculation by replacing the $\partial^2 X_{11}/\partial x^2$ term with $(\beta_{11}{}^{\mathrm{ad}})^2 X_{11}$, where $(\beta_{11}{}^{\mathrm{ad}})^2$ is the eigenvalue in Eq. (13). The N_y variational eigenfuctions $Y_j(y)$ are obtained by solving Eq. (15). The scalar separable effective adiabatic basis (SEAB) is given by multiplying the two sets $\{X_i(x)\}$ and $\{Y_j(y)\}$. The separable basis functions $\phi_l(x, y)$ are of the form $X_i(x)Y_j(y)$, where $i = 1,...,N_x$; $j = 1,...,N_y$; and $l = (j - 1)N_x + i$. A related method by which the modal field is obtained variationally as a separable function of the coordinates has been developed by Sharma *et al.*[15]

The separable basis functions $\{\phi_l(x, y)\}$ are sufficient to solve the scalar wave equation Eq. (11). It should be extended to be used as a basis in the variational solution of the vector Maxwell equation given in Eq. (4). However, we will discuss the properties of $\{\phi_l(x, y)\}$ before proceeding any further. Both sets $\{Y_j(y)\}$ and $\{X_i(x)\}$ are orthogonal, since they are solutions of the one-dimensional Hermitian eigenvalue problem. It follows that $\{\phi_l(x, y)\}$ is an orthogonal set, too. For the same reason, right and left functions $\phi_l(x, y)$ are connected by the complex conjugation. Notwithstanding the use of the Fourier basis in the solutions of Eqs. (12), (14), and (15), the use of the SEAB is a considerable improvement over

the direct application of the Fourier basis to Eq. (11) because $\{\phi_l(x, y)\}$ contains as many as N_xN_y different Fourier components. This number can be larger than 10^6. Therefore it requires the construction of matrices with huge dimensionality, which are hard or even impossible to diagonalize with the available computational facilities.

The solutions of the vector equation (4) are the functions that consist of two components $\mathbf{E}_\perp(x, y) = [E_x(x, y), E_y(x, y)]$. We represent these functions in a basis $\{\mathbf{E}_k(x, y):[0, \phi_l(x, y)], [\phi_l(x, y), 0]\}$, where $l = 1,...N$; the vector basis function index, k, assumes values from 1 to $2N$. N is a cutoff in the number of the basis functions. With this basis, we form the operator $\hat{\Theta}$, represented by a matrix whose elements are given by

$$\Theta_{kl} = \int \mathrm{d}x\mathrm{d}y \mathbf{E}_k^{\dagger}(x, y)\hat{\Theta}\mathbf{E}_l(x, y), \tag{17}$$

where $\mathbf{E}_k^{\dagger}(x, y)$ is a Hermitian-adjoint vector. With the choice of an appropriate numerical procedure, matrix (17) can be diagonalized.

We note here that evaluation of the matrix elements of $\hat{\Theta}$ is a time-consuming procedure when the refractive index, $n(x, y)$, varies continuously. However, in the waveguides with a step-index profile, derivatives of $f(x, y) = 2 \ln n(x, y)$ are just a delta function or its derivatives. Thus, in this case, numerical work will amount to evaluation of one-dimensional integrals along the curves where the discontinuity of the refractive index occurs. An example of the resulting matrix elements is given in Appendix A.

We give a summary of the steps by which SEAB functions are calculated. First, Eq. (12) is solved to obtain $n_1(x)$, the effective refractive index of the media in the x direction. Second, Eq. (14) is solved to obtain x-dependent functions $X_i(x)$. Third, the effective refractive index of the media in the y direction, $n(y)$, is obtained from Eq. (16). As the last step, Eq. (15) is solved for $Y_j(y)$, the y-dependent part of the basis.

5. ILLUSTRATIVE NUMERICAL EXAMPLE AND DISCUSSION

We demonstrate here the efficiency of the adiabatic basis by comparing the solution of the scalar wave equation in terms of this basis with the solutions obtained when the primitive sine basis was used. Alternatively, one may use Hermite–Gauss functions as a basis set and not sine functions. For example, when $n(x, y)^2$ is close to the harmonic potential, the convergence to the exact numerical solution will be faster with the Hermite–Gauss basis functions than with the sine basis. However, in cases in which $n(x, y)^2$ is a finite rectangular well, i.e., very anharmonic, we expect that the use of the sine basis will lead to faster convergence than the Hermite–Gauss basis will. The sine basis is also superior to the Hermite–Gauss functions in calculations of leaky modes. Another benefit of the sine basis is that matrix elements for the step-function refraction index can be evaluated analytically. The sine basis is given by

$$\phi_l^{\sin}(x, y) = \frac{2}{(L_xL_y)^{1/2}} \sin\left(\frac{2\pi i}{L_x}x\right) \sin\left(\frac{2\pi j}{L_y}y\right), \tag{18}$$

where L_x and L_y are box dimensions and $l = (j - 1)N_x + i$, $i = 1...N_x$, and $j = 1...N_y$. Computations of the effective index, $n_{\mathrm{eff}} = \beta/k$, were carried out in two common structures: a single-mode rectangular waveguide and a multimode rib waveguide. Since the scalar wave equation is a Hermitian eigenvalue problem, we know that the variational eigenvalues are lower bounds of the exact values. A reasonable estimate of computational error is given by the increment in the effective index as the number of the basis functions is increased. For the waveguides analyzed in this paper, the Hermite–Gauss basis can be a better choice, as we noted in Section 1. However, in comparing the SEAB with the sine basis, we had in mind its future application to waveguides with cross sections of such complexity as to render the use of the Hermite–Gauss basis impractical.

We choose the rectangular waveguide dimensions to be 4 μm × 1 μm, with $n_{\mathrm{core}} = 1.495$ and $n_{\mathrm{clad}} = 1.445$. The core rests on a 9-$\mu$m-thick SiO_2 substrate, and the top cladding is 6 μm thick. Above the top cladding, there is

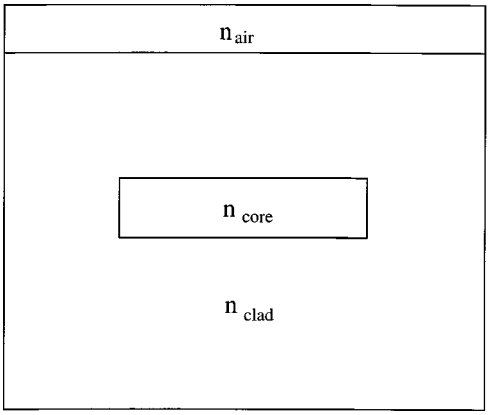

Fig. 1. Schematic drawing of the rectangular single-mode waveguide. Waveguide dimensions are 4 μm × 1 μm, $n_{\mathrm{core}} = 1.495$, $n_{\mathrm{clad}} = 1.445$, bottom cladding of 9 μm, top cladding of 6 μm, and $\lambda = 1.55$ μm.

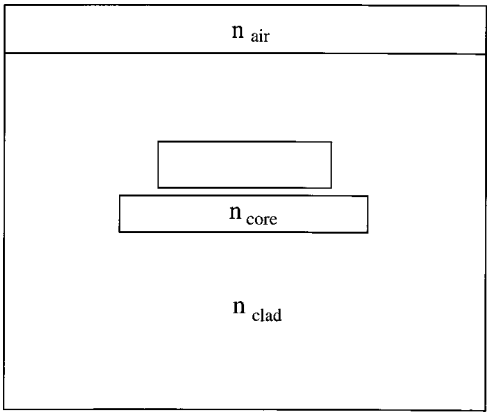

Fig. 2. Schematic drawing of the rib waveguide. The first core layer is 12 μm × 0.6 μm, the second core layer is 8 μm × 1.5 μm, and the intermediate cladding layer is 0.2 μm. The rest of the parameters are in the caption to Fig. 1.

Table 1. Effective Refractive Index, n_{eff}, and the Computation Error of the Scalar Wave Equation Solution in the Single-Mode Rectangular Waveguide[a]

Number of Basis Functions, $\phi_l = X_i(x)Y_j(y)$	Sine Basis		Adiabatic Basis	
	n_{eff}	Error	n_{eff}	Error
$i_{\max} = 40, j_{\max} = 10, l_{\max} = 400$	1.453523	—	1.457050	—
$i_{\max} = 60, j_{\max} = 15, l_{\max} = 900$	1.455190	1.667×10^{-3}	1.457102	5.2×10^{-5}
$i_{\max} = 80, j_{\max} = 20, l_{\max} = 1600$	1.456160	9.70×10^{-4}	1.457141	3.9×10^{-5}
$i_{\max} = 100, j_{\max} = 25, l_{\max} = 2500$	1.456459	2.99×10^{-4}	1.457152	1.1×10^{-5}

[a] In the case of the sine basis, $\Phi_i(x)\Psi_j(y)$ corresponds to the functions in Eq. (18); in the case of the adiabatic basis, they are defined in Eqs. (14) and (15).

Table 2. Effective Refractive Index; n_{eff}, and the Computation Error of the First Bound Mode in the Rib Waveguide[a]

Number of Basis Functions, $\phi_l = X_i(x)Y_j(y)$	Sine Basis		Adiabatic Basis	
	n_{eff}	Error	n_{eff}	Error
$i_{\max} = 40, j_{\max} = 10, l_{\max} = 400$	1.471733	—	1.473935	—
$i_{\max} = 60, j_{\max} = 15, l_{\max} = 900$	1.473420	1.687×10^{-3}	1.473947	1.2×10^{-5}
$i_{\max} = 80, j_{\max} = 20, l_{\max} = 1600$	1.473587	1.67×10^{-4}	1.473950	3×10^{-6}
$i_{\max} = 100, j_{\max} = 25, l_{\max} = 2500$	1.473691	1.04×10^{-4}	1.473952	2×10^{-6}

[a] For the definition of $\Phi_i(x)\Psi_j(y)$, see the caption to Table 1.

Table 3. Effective Refractive Index, n_{eff}, and the Computation Error of the Last Bound Mode in the Rib Waveguide[a]

Number of Basis Functions, $\phi_l = X_i(x)Y_j(y)$	Sine Basis		Adiabatic Basis	
	n_{eff}	Error	n_{eff}	Error
$i_{\max} = 40, j_{\max} = 10, l_{\max} = 400$	1.444219	—	1.445291	—
$i_{\max} = 60, j_{\max} = 15, l_{\max} = 900$	1.444364	1.45×10^{-4}	1.445351	6.0×10^{-5}
$i_{\max} = 80, j_{\max} = 20, l_{\max} = 1600$	1.444693	3.29×10^{-4}	1.445376	2.5×10^{-5}
$i_{\max} = 100, j_{\max} = 25, l_{\max} = 2500$	1.444741	4.8×10^{-5}	1.445386	1.0×10^{-5}

[a] Note that this state is found to be bound only when the adiabatic basis is used. For the definition of $\Phi_i(x)\Psi_j(y)$, see the caption to Table 1.

an air layer. We choose $L_x = 100\ \mu$m, $L_y = 20\ \mu$m, and $N_x = N_y = 512$. The wavelength in vacuum is $\lambda = 1.55\ \mu$m (see Fig. 1). We quote the results in Table 1.

We notice that the results obtained with the adiabatic basis set have an error that is approximately 20 times smaller than the error incurred when the sine basis is used. The results obtained with both basis sets depend weakly on the box dimensions.

In addition, we present calculations of n_{eff} in a multimode rib waveguide (see Fig. 2). The first core layer is $12\ \mu\text{m} \times 0.6\ \mu$m, and the second one is $8\ \mu\text{m} \times 1.5\ \mu$m. The width of the SiO_2 layer between the two core layers is $0.2\ \mu$m. Its purpose is to facilitate convergence of the calculations for the bound states. It is known[16] that numerical solutions of the wave equation inside polygons containing vertices with angles greater than π are, in general, poorly convergent. It should be stressed, however, that, since $\lambda \gg 0.2\ \mu$m, this thin layer does not alter the modal structure of the propagated light. The rest of the parameters is the same as in the case of the rectangular waveguide considered previously.

For the multimode rib waveguide, solutions obtained with the adiabatic basis functions provide five bound (trapped) modes, the last of which is located very close to the threshold. Use of the sine basis yields only four bound modes, which illustrates the poor convergence of this method near the threshold. We quote the convergence of the first and the last bound modes in Tables 2 and 3. The bound (trapped) modes are ordered according to the number of nodes. This illustrates the numerical advantage of using our method to calculate weakly bound (trapped) modes.

In the case of the first bound mode, the error ratio is close to that found in the single-mode rectangular waveguide; the adiabatic basis proves again to be superior to the sine basis. In the case of the last bound mode, we see that the error ratio is smaller. That is a consequence of the Ritz variational method, whose error increases with the mode's number. Despite this, adiabatic basic functions still seem a much better choice.

To illustrate the fact that the use of the SEAB rather than the primitive sine functions reduces the computational effort that is required to obtain converged results, we define the following error estimate: If $\Sigma_i^N a_i \phi_i$ is the variational eigenfunction and ϕ_i are N basis functions, then the error can be represented as

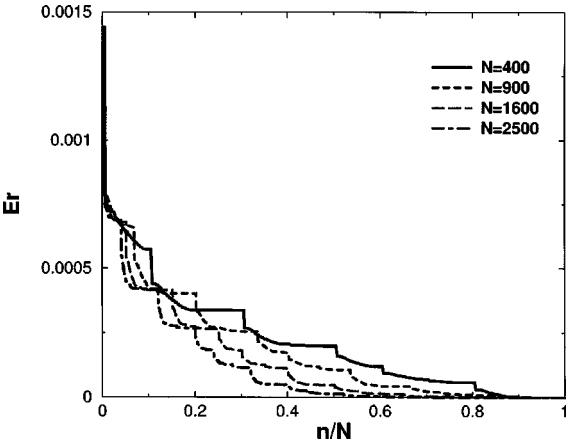

Fig. 3. Error estimate [see Eq. (19)] in the computation of the first bound mode of the rib waveguide (see Fig. 2) by the SEAB.

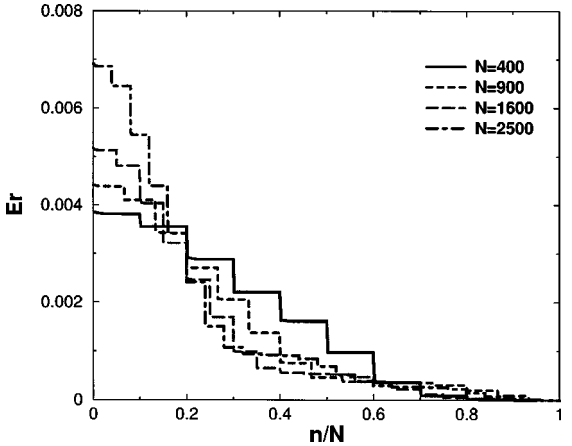

Fig. 4. Error estimate [see Eq. (19)] in the computation of the first bound mode of the rib waveguide (see Fig. 2) by the sine basis.

$$\mathrm{Er}(n) = 1 - \sum_{i}^{n} |a_i|^2, \tag{19}$$

where $n = 1,...,N$. In Figs. 3 and 4 we plot $\mathrm{Er}(n)$ obtained in the calculation of the first bound mode of the rib waveguide (see Fig. 2) with the SEAB and sine basis functions, respectively.

Function $\mathrm{Er}(n)$ gives an estimate of the rate of convergence of the variational calculation. We see from Figs. 3 and 4 that approximately ten SEAB functions are necessary to obtain 99.9% of the variational function, whereas several hundred primitive sine basis functions are needed to achieve the same result. The larger the rate of convergence is, the faster variational eigenfunctions approach a numerically exact solution.

To calculate the quasi-TE (x-polarized) and quasi-TM (y-polarized) modes in the waveguide structures presented above, we diagonalize the matrix Θ_{ij}, given in Eq. (17) (obtained in the adiabatic basis). The resulting matrix was not Hermitian; thus the generalized diagonalization LAPACK procedure was used to recover the eigenvalues and the left and right eigenvectors of Θ_{ij}. The complex parts of the propagation constants were found to be much smaller than the computational error and were subsequently neglected. This result indicates that the approximation made in Eqs. (4) and (5) was valid for the systems investigated in this paper. We quote the propagation constants of the TE and TM modes in Tables 4–6; it is interesting to note that the error involved in calculations is much smaller than the geometrical birefringence [i.e., $n_{\mathrm{eff}}(\mathrm{TE}) - n_{\mathrm{eff}}(\mathrm{TM})$] for an adiabatic basis as small as 400 functions.

Right eigenvectors of Θ_{ij} represent the electric field distribution across the cross section of the waveguide. Calculated modes are given in the form of vectors $\mathbf{E}_{\perp} = [E_x(x, y), E_y(x, y)]$. We can still easily characterize the solutions as TE or TM, since the power carried by the mode is concentrated mostly in the $E_x(x, y)$ or $E_y(x, y)$

Table 4. Results of the Full Vectorial Calculations for the Single-Mode Rectangular Waveguide[a]

Number of Basis Functions, $\phi_l = X_i(x)Y_j(y)$	TM Mode		TE Mode	
	n_{eff}	Error	n_{eff}	Error
$i_{\max} = 40, j_{\max} = 10, l_{\max} = 400$	1.457153	—	1.457942	—
$i_{\max} = 60, j_{\max} = 15, l_{\max} = 900$	1.457205	5.2×10^{-5}	1.458009	6.7×10^{-5}
$i_{\max} = 80, j_{\max} = 20, l_{\max} = 1600$	1.457249	4.4×10^{-5}	1.458057	4.8×10^{-5}

[a] Note that the number of basis functions is actually twice the number given in this and subsequent tables owing to the vectorial nature of solutions. Note that the actual number of vector basis functions $\mathbf{E}_k(x, y)$ is $2l_{\max}$.

Table 5. Results of the Full Vectorial Calculations of the First Bound Mode in the Rib Waveguide[a]

Number of Basis Functions, $\phi_l = X_i(x)Y_j(y)$	TM Mode		TE Mode	
	n_{eff}	Error	n_{eff}	Error
$i_{\max} = 40, j_{\max} = 10, l_{\max} = 400$	1.473997	—	1.474862	—
$i_{\max} = 60, j_{\max} = 15, l_{\max} = 900$	1.474012	1.5×10^{-5}	1.474872	1.0×10^{-5}
$i_{\max} = 80, j_{\max} = 20, l_{\max} = 1600$	1.474016	4×10^{-6}	1.474875	3×10^{-6}

[a] Note that the actual number of vector basis functions $\mathbf{E}_k(x, y)$ is $2l_{\max}$.

Table 6. Results of the Full Vectorial Calculations of the Last Bound Mode in the Rib Waveguide[a]

Number of Basis Functions, $\phi_l = X_i(x)Y_j(y)$	TM Mode		TE Mode	
	n_{eff}	Error	n_{eff}	Error
$i_{\max} = 40, j_{\max} = 10, l_{\max} = 400$	1.445297	—	1.445421	—
$i_{\max} = 60, j_{\max} = 15, l_{\max} = 900$	1.445361	6.4×10^{-5}	1.445499	7.8×10^{-5}
$i_{\max} = 80, j_{\max} = 20, l_{\max} = 1600$	1.445387	2.6×10^{-5}	1.445533	3.4×10^{-5}

[a] Note that the actual number of vector basis functions $\mathbf{E}_k(x, y)$ is $2l_{\max}$.

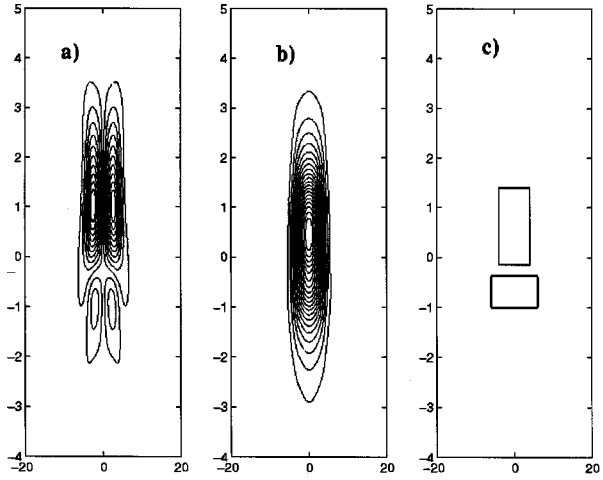

Fig. 5. Real part of the first bound TM mode of the rib waveguide. a) E_x, subdominant component; b) E_y, dominant component; c) waveguide's sketch.

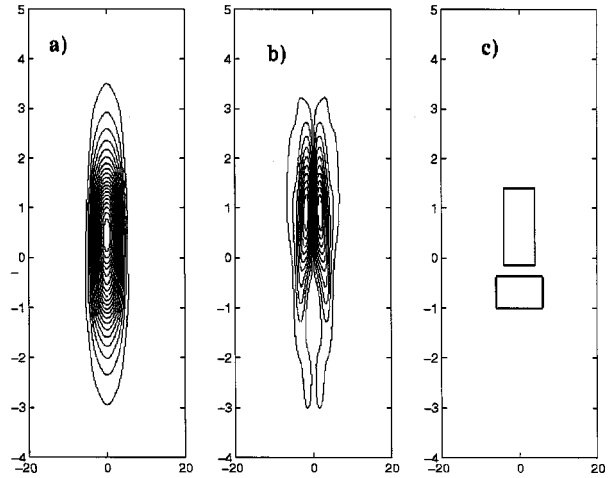

Fig. 6. Real part of the first TE mode of the rib waveguide. a) E_x, dominant component; b) E_y, subdominant component; c) waveguide's sketch.

component, respectively. Indeed, we found that for the structures under question the power contained in the dominant component is larger than the power contained in the subdominant component by factor of 10^5. We found also that the complex parts of both dominant and subdominant components of TE–TM modes were several orders of magnitude smaller than the corresponding real parts. Thus the modal field is linearly polarized with the direction of polarization varying across the cross section.

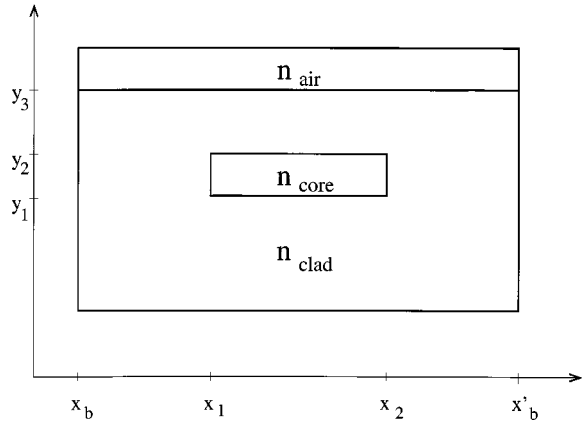

Fig. 7. Representative waveguide with a step-index profile used to demonstrate the calculation of matrix elements of $\hat{\Theta}$. Coordinates x_i and y_j mark the position of intervals at which the change in the refractive index takes place.

We show a representative field distribution for the ground TE and TM modes of the rib waveguide in Figs. 5 and 6.

It is known that across the surfaces separating media with indices of refraction n_1 and n_2 the normal component of the electric field is discontinuous. The relation between the fields on either side of the interface is the following: $E_1 {n_1}^{1/2} = E_2 {n_2}^{1/2}$. There is a legitimate question of how well the continuous basis function can describe the resulting finite jump in the field amplitude. We observed no field discontinuities in the current investigation that can be explained in the following way. In the waveguides under investigations, the field jump across the core–cladding interface is only 1.5% of the field strength there. And although the jump in the normal component is approximately 20% across the cladding–air interface, the field of the bound modes is exponentially small there. Moreover, to obtain the SEAB we introduce a grid to perform numerical integrations; thus the solutions are given on the grid and therefore smoothed. To give a satisfactory answer to the question above, additional investigation in a suitably chosen waveguide and sufficiently dense grid should be carried out. However, this is outside the scope of the present paper.

6. CONCLUSIONS

In this paper we demonstrated a novel efficient method of solution of the transverse vector wave equation. A separable effective adiabatic basis set was constructed and used as a variational basis set. We demonstrate that the use of effective adiabatic basis functions permits the cal-

culation of the waveguide's modes with a very high accuracy even for the small number of basis functions. Another useful feature of our approach is that this optimal basis should not be chosen *a priori*, but it can be computed numerically for waveguides with any cross section. Computation of scalar modes in single-mode rectangular and multimode rib waveguides clearly showed that the effective adiabatic basis is much superior to the commonly used Fourier or sine basis. Computation of the TE and TM vector modes had an error that was much smaller than the birefringence even for a moderate number of basis functions.

APPENDIX A: MATRIX ELEMENTS

In this appendix we present the matrix elements of $\hat{\Theta}$ for the representative waveguide structure (see Fig. 7). We assume that the waveguide has step-function refractive-index profiles, with the boundaries between regions of different refractive indices parallel to either the x or the y axis. We denote the effective adiabatic basis set by

$$\mathbf{E}_l^{(x)}(x, y) = (X_i Y_j, 0),$$
$$\mathbf{E}_l^{(y)}(x, y) = (0, X_i Y_j), \tag{A1}$$

where X_i and Y_j are defined in the text in Eqs. (14) and (15). We see that half of the basis functions are polarized in the x direction, and the second half are the y-polarized functions. We will refer to $\mathbf{E}_\perp^{(x)}(x, y)$ and $\mathbf{E}_\perp^{(y)}(x, y)$ as x-polarized and y-polarized bases, respectively.

We report here only the matrix elements of the second term of $\hat{\Theta}$ in Eq. (5), which is denoted below as $\hat{V}$:

$$\hat{V} = \begin{bmatrix} f_x \dfrac{\partial}{\partial x} + f_{xx} & f_y \dfrac{\partial}{\partial x} + f_{xy} \\ f_x \dfrac{\partial}{\partial y} + f_{xy} & f_y \dfrac{\partial}{\partial y} + f_{yy} \end{bmatrix}, \tag{A2}$$

since the first term can be handled in an elementary way. Calculation of the matrix elements is comparatively easy, since for the step-index profile derivatives of $f = 2 \ln n(x, y)$ are reduced to some functions that contain either the delta function or its derivative. As a result, integrals involved in the evaluation of these matrix elements should be computed only along the intervals in which the change in the refractive index takes place. Thus we obtain the following matrix elements.

(a) Matrix element calculated with two x-polarized functions $\mathbf{E}_l^{(x)}(x, y) = (X_k Y_i, 0)$ and $\mathbf{E}_m^{(x)}(x, y) = (X_l Y_j, 0)$:

$$V_{lm}^{(xx)} = [\mathbf{E}_l^{(x)} | \hat{V} | \mathbf{E}_m^{(x)}] = 4 \sum_{p=1}^{2} \left[\int_{y_{\mathrm{in}}(x_p)}^{y_{\mathrm{fin}}(x_p)} dy\, Y_i^*(y) Y_j(y) \right] \frac{n(x_{p^+}, y) - n(x_{p^-}, y)}{n(x_{p^+}, y) + n(x_{p^-}, y)} \left[\frac{dX_k^*(x)}{dx} X_l(x) \right] \Bigg|_{x=x_p}. \tag{A3}$$

By $y_{\mathrm{in}}(x_p)$ and $y_{\mathrm{fin}}(x_p)$ we denote the initial and final points of the interval located at $x = x_p$. For example, for $x = x_1$: $y_{\mathrm{in}}(x_1) = y_1$, $y_{\mathrm{fin}}(x_1) = y_2$; for $x = x_2$: $y_{\mathrm{in}}(x_2) = y_1$, $y_{\mathrm{fin}}(x_2) = y_2$ (see Fig. 7).

(b) Analogously, the matrix element calculated with two y-polarized functions $\mathbf{E}_l^{(y)}(x, y) = (0, X_i Y_k)$ and $\mathbf{E}_m^{(y)}(x, y) = (0, X_j Y_l)$:

$$V_{lm}^{yy} = [\mathbf{E}_l^{(y)} | \hat{V} | \mathbf{E}_m^{(y)}] = 4 \sum_{p=1}^{3} \left[\int_{x_{\mathrm{in}}(y_p)}^{x_{\mathrm{fin}}(y_p)} dx X_i^*(x) X_j(x) \right] \frac{n(x, y_{p^+}) - n(x, y_{p^-})}{n(x, y_{p^+}) + n(x, y_{p^-})} \left[\frac{dY_k^*(y)}{dy} Y_l(y) \right] \Bigg|_{y=y_p}, \tag{A4}$$

where, for example, $x_{\mathrm{in}}(y_1) = x_1$ and $x_{\mathrm{fin}}(y_1) = x_2$, $x_{\mathrm{in}}(y_2) = x_1$ and $x_{\mathrm{fin}}(y_2) = x_2$, and $x_{\mathrm{in}}(y_3) = x_b$ and $x_{\mathrm{fin}}(y_3) = x_b'$ (see Fig. 7).

(c) Matrix element calculated with x-polarized function $\mathbf{E}_l^{(x)}(x, y) = (X_i Y_k, 0)$ and y-polarized function $\mathbf{E}_m^{(y)}(x, y) = (0, X_j Y_l)$:

$$V_{lm}^{(xy)} = [\mathbf{E}_l^{(x)} | \hat{V} | \mathbf{E}_m^{(y)}] = 4 \sum_{p=1}^{3} \left[\int_{x_{\mathrm{in}}(y_p)}^{x_{\mathrm{fin}}(y_p)} dx X_i^*(x) \frac{dX_j}{dx}(x) \right] \frac{n(x, y_{p^+}) - n(x, y_{p^-})}{n(x, y_{p^+}) + n(x, y_{p^-})} [Y_k^*(y) Y_l(y)] \big|_{y=y_p}. \tag{A5}$$

(d) Matrix element calculated with y-polarized function $\mathbf{E}_l^{(y)}(x, y) = (0, X_k Y_i)$ and x-polarized function $\mathbf{E}_m^{(x)}(x, y) = (X_l Y_j, 0)$:

$$V_{lm}^{(yx)} = [\mathbf{E}_l^{(y)} | \hat{V} | \mathbf{E}_m^{(x)}] = 4 \sum_{p=1}^{2} \left[\int_{y_{\mathrm{in}}(x_p)}^{y_{\mathrm{fin}}(x_p)} dy\, Y_i^*(y) \frac{dY_j}{dy}(y) \right] \frac{n(x_{p^+}, y) - n(x_{p^-}, y)}{n(x_{p^+}, y) + n(x_{p^-}, y)} [X_k^*(x) X_l(x)] \big|_{x=x_p}. \tag{A6}$$

ACKNOWLEDGMENT

The authors thank R. Narevich from Optun Ltd. for his invaluable help during the preparation of this study.

N. Moiseyev and K. Gokhberg, the corresponding authors, can be reached by e-mail at nimrod@technion.ac.il and at kirill@pci.uni-heidelberg.de.

REFERENCES

1. K. S. Chiang, C. H. Kwan, and K. M. Lo, "Effective-index method with built-in perturbation correction for the vector modes of rectangular-core optical waveguides," J. Lightwave Technol. **17**, 716–722 (1999).

2. C. H. Kwan and K. S. Chiang, "Study of polarization-dependent coupling in optical waveguide directional couplers by the effective-index method with built-in perturbation correction," J. Lightwave Technol. **20**, 1018–1026 (2002).
3. W. Huang, H. A. Haus, and H. N. Yoon, "Analysis of buried-channel waveguides and couplers: scalar solution and polarization correction," J. Lightwave Technol. **8**, 642–648 (1990).
4. W. Huang and H. A. Haus, "A simple variational approach to optical rib waveguides," J. Lightwave Technol. **9**, 56–61 (1991).
5. C. H. Henry and B. H. Verbeek, "Solution of the scalar wave equation for arbitrarily shaped dielectric waveguides by two-dimensional Fourier analysis," J. Lightwave Technol. **7**, 308–313 (1989).
6. M. A. Forastiere and G. C. Righini, "Scalar analysis of general dielectric waveguides by Fourier decomposition method," J. Lightwave Technol. **17**, 362–368 (1999).
7. K. M. Lo and E. H. Li, "Solutions of the quasi-vector wave equation for optical waveguides in a mapped infinite domains by the Galerkin's method," J. Lightwave Technol. **16**, 937–944 (1998).
8. R. L. Gallawa, I. C. Goyal, Y. Tu, and A. K. Ghatak, "Optical waveguide modes: an approximate solution using Galerkin's method with Hermite–Gauss basis functions," IEEE J. Quantum Electron. **27**, 518–522 (1991).
9. T. Rasmussen, J. H. Povlsen, A. Bjarklev, O. Lumholt, B. Pedersen, and K. Rottwit, "Detailed comparison of two approximate methods for the solution of the scalar wave equation for a rectangular optical waveguide," J. Lightwave Technol. **11**, 429–433 (1993).
10. M. V. Berry, "Quantum adiabatic anholonomy" in *Anomalies, Phases, Defects*, U. M. Bregola, G. Marmo, and G. Morandi, eds. (Bibliopolis, Naples, Italy, 1990), pp. 125–181.
11. A. Yariv, *Optical Electronics*, 3rd ed. (CBS College, New York, 1985).
12. N. Moiseyev, "Quantum theory of resonances," Phys. Rep. **302**, 212–293 (1998).
13. R. März, *Integrated Optics* (Artech House, Norwood, Mass., 1995).
14. A. S. Davydov, *Quantum Mechanics* (Pergamon, New York, 1965).
15. A. Sharma, "Analysis of integrated optical waveguides: variational method and effective-index method with built-in perturbation correction," J. Opt. Soc. Am. A **18**, 1383–1387 (2001).
16. J. R. Kuttler and V. G. Sigillito, "Eigenvalues of the Laplacian in two dimensions," SIAM Rev. **26**, 163–193 (1984).